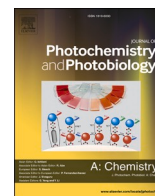




Contents lists available at ScienceDirect

## Journal of Photochemistry &amp; Photobiology, A: Chemistry

journal homepage: [www.elsevier.com/locate/jphotochem](http://www.elsevier.com/locate/jphotochem)

## Helical aggregates of bis(styryl) dyes formed by DNA templating

Maria A. Ustimova<sup>a,\*</sup>, Yury V. Fedorov<sup>a</sup>, Vladimir B. Tsvetkov<sup>b</sup>, Sergey D. Tokarev<sup>a</sup>, Nikolai A. Shepel<sup>a</sup>, Olga A. Fedorova<sup>a</sup>

<sup>a</sup> Laboratory of Photoactive Supramolecular Systems, A.N. Nesmeyanov Institute of Organoelement Compounds of Russian Academy of Sciences, Vavilova St. 28, Moscow, 119991, Russia

<sup>b</sup> WCRC "Digital biodesign and personalized healthcare", Sechenov First Moscow State Medical University, Trubetskaya St. 8/2, Moscow, 119146, Russia

## ARTICLE INFO

## Keywords:

Bisstyryl dye  
DNA  
Aggregate  
Groove binding  
FRET

## ABSTRACT

In order to further investigate mechanism of the styryl dye – DNA interaction, three different bis(styryl)pyridinium dyes possessing OMe or/and NMe<sub>2</sub> substituents in phenyl ring were selected and interaction of these compounds with the calf thymus DNA (ct-DNA) was monitored by using of UV–vis and fluorescence spectroscopic techniques, circular dichroism (CD), Hoechst 33258 displacement experiments and quantum-chemical calculations. The experimental results indicated a higher fluorescence enhancement for dyes containing NMe<sub>2</sub> group upon binding with DNA. The results proved the interaction of the molecules with ct-DNA occurs through the formation of aggregates in minor groove at high dye concentration. Bis(styryl) dye with OMe substituent forms the helical dye aggregates of right-handed chirality, whereas, dye containing NMe<sub>2</sub> group demonstrates formation of left-handed chiral aggregates in minor groove of DNA. As the DNA concentration increases, the dyes begin to spread out along the minor groove. This research provided a better understanding of mechanism of styryl dye - DNA interaction and effect of dye structure on interacting mode with DNA.

## 1. Introduction

The spontaneous noncovalent assembly of cyanine dyes within the minor groove of ds DNA causes the formation of helical dye aggregates in the DNA template which differ in the size and shape [1–5]. The formed well-defined aggregates exhibit induced chirality and interesting optical properties. A second feature arising from the noncovalent assembly is that dimerization is highly selective for A-T sequences over G-C [6]. One important advantage of these aggregates is that their structure and size can be controlled by the DNA template.

Binding of cyanine dyes to DNA can occur with significant fluorescence enhancement due to restricted internal rotation upon binding to nucleic acid [7]. Thus, a variety of dyes based on benzoxazole, benzothiazole, quinolone, pyridine heterocycles exhibits the increase of the fluorescence intensity up to 260-fold upon binding to calf thymus DNA [8–10].

Another well-studied example is binding of DNA to the natural product distamycin [11–15]. This compound binds as a face-to-face dimer in the minor groove of certain DNA sequences, including alternating A-T sequences.

The selectivity, sensitivity and binding properties of the mono- and

bis(styryl) dyes interacting with DNAs have been also investigated [16–25]. Dyes exhibit the properties of long-wave emission, large Stokes shifts, water solubility, and large fluorescent enhancement towards nucleic acids. The formation of aggregates within the minor groove of double stranded DNA is less studied compared to cyanine dyes. Two reports mentioned of styryl dye aggregates have been found in literature. Thus, for the 4-alkoxystyryl(pyridinium) dye series, the presence of the second DNA-binding unit led to the minor groove binding accompanied by the aggregation [26]. Bis(styryl) dyes, in which two styrylpyridine moieties are connected to each other through the oxo- or azacrown ether unit and constructing in tail-to-tail mode, at low DNA concentration form the aggregates located in minor groove [27]. Also analysis of the dye-DNA binding results demonstrated that crown ether macrocycle included in the dye is localized near G-C pairs through the hydrogen bonds.

In this study, we investigated the effect of substituents in bis(styryl) pyridine dyes **1a**, **b**, **2** on the formation of aggregates in DNA template and fluorescent response on binding with DNA. In the composition of dyes the substituents in the phenyl ring were OMe or/and NMe<sub>2</sub> groups.

\* Corresponding author.

E-mail addresses: [ustimova.maria@yandex.ru](mailto:ustimova.maria@yandex.ru) (M.A. Ustimova), [fedorova@ineos.ac.ru](mailto:fedorova@ineos.ac.ru) (O.A. Fedorova).

<https://doi.org/10.1016/j.jphotochem.2021.113378>

Received 22 March 2021; Received in revised form 13 May 2021; Accepted 19 May 2021

Available online 21 May 2021

1010-6030/© 2021 Elsevier B.V. All rights reserved.

## 2. Experimental section

### 2.1. General methods

$^1\text{H}$  NMR spectra were recorded at 400 MHz, and  $^{13}\text{C}$  NMR spectra were recorded at 101 or 151 MHz at ambient temperature using 5 mm tubes. Chemical shifts were determined with the accuracy of 0.01 and 0.1 ppm for  $^1\text{H}$  and  $^{13}\text{C}$  spectra, respectively, and are given relative to the residual signal of the solvent that was used as an internal reference. The coupling constants were determined with the accuracy of 0.1 Hz. Electrospray ionization (ESI) mass spectra were detected in the mode of full mass scanning of positive ions on a tandem dynamic mass spectrometer equipped with a mass analyzer with an octapole ionic trap. Melting points were measured on Melt-temp melting point electrothermal apparatus and were uncorrected. Elemental analysis was performed on the Carlo Erba 1108 elemental analyzer at the Laboratory of Microanalysis of A. N. Nesmeyanov Institute of Organoelement Compounds of RAS, Moscow, Russia.

### 2.2. Synthesis of the compounds 1a,b, 2, 5a,b

4-[4-(Methoxy)styryl]pyridine 3a [28], 4-[4-(dimethylamino)styryl]pyridine 3b [29], (E)-4-[4-(methoxy)styryl]-1-methylpyridinium iodide 5a and (E)-4-[4-(dimethylamino)styryl]-1-methylpyridinium iodide 5b [30] were prepared by literature procedures. All other reagents and solvents were obtained from commercial sources and used as received.

#### 2.2.1. General procedure for the synthesis of bis-styryl 1a and 1b

A mixture of styrylpyridine 3a or 3b (0.47 mmol) and dibromopropane (0.235 mmol) in DMF (5 mL) was stirred at 80 °C for 24 h. After being cooled at room temperature, 10 mL ethyl acetate was added and the precipitate was filtered off. The precipitate was washed with hexanes and ethyl acetate and dried.

#### 2.2.2. (E)-1,1'-(propane-1,3-diyl)bis(4-(4-methoxystyryl)pyridinium) bromide (1a)

Yellow solid, yield 36 %, m.p. 256–258 °C.  $^1\text{H}$  NMR (400 MHz,  $\text{CD}_3\text{CN}$ ): 2.67 (m, 1H, H- $\omega$ ); 3.84 (s, 3H,  $\text{CH}_3$ ); 4.68 (t, 2H, H- $\beta$ ,  $J = 6.9$ , 6.8); 7.01 (d, 2H, H-9, H-11,  $J = 8.8$ ); 7.21 (d, 1H, b,  $J_{\text{trans}} = 16.2$ ); 7.66 (d, 2H, H-8, H-12,  $J = 8.8$ ); 7.81 (d, 1H, a,  $J_{\text{trans}} = 16.2$ ); 7.98 (d, 2H, H-3, H-5,  $J = 6.9$ ); 8.77 (d, 2H, H-2, H-6,  $J = 6.9$ ).  $^{13}\text{C}$  NMR (400 MHz,  $\text{CD}_3\text{CN}$ ): 32.0 (C- $\omega$ ), 55.3 ( $\text{CH}_3$ ), 56.7 (C- $\beta$ ), 114.6 (C-9, C-11), 120.2 (C-b), 123.7 (C-3, C-5), 127.4 (C-7), 130.2 (C-8, C-12), 141.8 (C-a), 143.9 (C-2, C-6), 154.6 (C-4), 162.0 (C-10). Anal. calcd for  $\text{C}_{31}\text{H}_{32}\text{Br}_2\text{N}_2\text{O}_2$ : C, 59.63; H, 5.17; N, 4.49; found: C, 59.65; H, 5.12; N, 4.45. ESI-MS 1a in  $\text{H}_2\text{O}$ ,  $m/z$ : calcd 232.3; found 232.9 [1a] $^{2+}$ .

#### 2.2.3. (E)-1,1'-(propane-1,3-diyl)bis(4-(4-(dimethylamino)styryl)pyridinium) bromide (1b)

Red solid, yield 33 %, m.p. 176–178 °C (dec.).  $^1\text{H}$  NMR (400 MHz,  $\text{CD}_3\text{CN}$ ): 2.55 (m, 1H, H- $\omega$ ); 3.04 (s, 6H,  $\text{CH}_3$ ); 4.44 (t, 2H, H- $\delta$ ,  $J = 7.6$ , 7.3); 6.76 (d, 2H, H-9', H-11',  $J = 8.9$ ); 7.02 (d, 1H, b',  $J_{\text{trans}} = 16.2$ ); 7.57 (d, 2H, H-8', H-12',  $J = 8.9$ ); 7.77 (d, 1H, a',  $J_{\text{trans}} = 15.9$ ); 7.85 (d, 2H, H-3', H-5',  $J = 6.9$ ); 8.33 (d, 2H, H-2', H-6',  $J = 6.7$ ).  $^{13}\text{C}$  NMR (400 MHz,  $\text{CD}_3\text{CN}$ ): 31.2 (C- $\omega$ ), 39.0 ( $\text{CH}_3$ ), 56.2 (C- $\delta$ ), 111.6 (C-9', C-11'), 116.2 (C-b'), 122.0 (C-7'), 122.4 (C-3', C-5'), 130.2 (C-8', C-12'), 142.7 (C-2', C-6'), 143.1 (C-a'), 152.4 (C-4'), 154.9 (C-10'). Anal. calcd for  $\text{C}_{33}\text{H}_{38}\text{Br}_2\text{N}_4$ : C, 60.93; H, 5.89; N, 8.61; found: C, 60.98; H, 5.84; N, 8.58. ESI-MS 1b in  $\text{H}_2\text{O}$ ,  $m/z$ : calcd 245.3; found 245.3 [1b] $^{2+}$ .

#### 2.2.4. (E)-1-(3-bromopropyl)-4-(4-(dimethylamino)styryl)pyridinium bromide (4)

A solution of compound 1b (0.1 g, 0.45 mmol) in DMF (10 mL) was very slowly added dropwise to a solution of 1,3-dibromopropane (0.454 g, 2.25 mmol) in DMF (2 mL) under continuous stirring at 80 °C in the argon atmosphere. After the addition was completed the obtained

mixture was stirred at 80 °C during 4 h. After being cooled at room temperature, 5 mL ethyl acetate was added and the precipitate was filtered off. The precipitate was washed with cold methanol and hot ethyl acetate and dried. Red solid, yield 25 %, m.p. 168–172 °C (dec.).  $^1\text{H}$  NMR (400 MHz,  $\text{CD}_3\text{CN}$ ): 2.48 (m, 2H, H- $\omega$ ); 3.04 (s, 6H,  $\text{CH}_3$ ); 3.49 (t, 2H, H- $\beta$ ,  $J = 6.4$ , 6.4); 4.51 (t, 2H, H- $\delta$ ,  $J = 7.1$ , 7.1); 6.79 (d, 2H, H-9', H-11',  $J = 8.9$ ); 7.06 (d, 1H, b',  $J_{\text{trans}} = 16.1$ ); 7.58 (d, 2H, H-8', H-12',  $J = 8.9$ ); 7.77 (d, 1H, a',  $J_{\text{trans}} = 16.1$ ); 7.88 (d, 2H, H-3', H-5',  $J = 6.9$ ); 8.42 (d, 2H, H-2', H-6',  $J = 6.9$ ).  $^{13}\text{C}$  NMR (400 MHz,  $\text{CD}_3\text{CN}$ ): 28.6 (C- $\beta$ ), 32.6 (C- $\omega$ ), 39.0 ( $\text{CH}_3$ ), 57.8 (C- $\delta$ ), 111.7 (C-9', C-11'), 116.3 (C-b'), 122.1 (C-7'), 122.5 (C-3', C-5'), 130.1 (C-8', C-12'), 142.7 (C-a'), 143.1 (C-2', C-6'), 152.3 (C-10'), 154.7 (C-4'). Anal. calcd for  $\text{C}_{18}\text{H}_{22}\text{Br}_2\text{N}_2$ : C, 50.73; H, 5.2; N, 6.57; Br, 37.5; found C, 50.69; H, 5.25; N, 6.61. ESI-MS 4 in MeCN,  $m/z$ : calcd 345.1; found 345.1 [4] $^{+}$ .

#### 2.2.5. 4-(4-(dimethylamino)styryl)-1-(3-(4-(4-methoxystyryl)pyridinium-1-yl)propyl)pyridinium iodide bromide (2)

A mixture of styrylpyridine 4 (0.14 mmol), 3a (0.14 mmol) and KI (0.14 mmol) in MeCN (5 mL) was stirred at 80 °C for 100 h. After being cooled at room temperature the solvent was evaporated and the obtained residue was recrystallized from methanol, the precipitate was filtered off. The precipitate washed with hot ethyl acetate and dried. Red solid, yield 50 %, m.p. 195–198 °C.  $^1\text{H}$  NMR (400 MHz,  $\text{DMSO}-d_6$ ): 2.62 (m, 2H, H- $\omega$ ); 3.02 (s, 6H,  $\text{N}(\text{CH}_3)_2$ ); 3.83 (s, 3H,  $\text{OCH}_3$ ); 4.58 (t, 2H, H- $\delta$ ,  $J = 7.6$ , 7.6); 4.65 (t, 2H, H- $\beta$ ,  $J = 7.3$ , 7.3); 6.78 (d, 2H, H-9', H-11',  $J = 9.0$ ); 7.06 (d, 2H, H-9, H-11,  $J = 8.4$ ); 7.2 (d, 1H, b',  $J_{\text{trans}} = 16.0$ ); 7.39 (d, 1H, b,  $J_{\text{trans}} = 16.2$ ); 7.59 (d, 2H, H-8, H-12,  $J = 8.9$ ); 7.71 (d, 2H, H-8', H-12',  $J = 8.1$ ); 7.95 (d, 1H, a',  $J_{\text{trans}} = 16.0$ ); 8.03 (d, 1H, a,  $J_{\text{trans}} = 16.2$ ); 8.09 (d, 2H, H-3', H-5',  $J = 5.8$ ); 8.22 (d, 2H, H-3, H-5,  $J = 5.4$ ); 8.84 (d, 2H, H-2', H-6',  $J = 5.8$ ); 8.98 (d, 2H, H-2, H-6,  $J = 5.4$ ).  $^{13}\text{C}$  NMR (400 MHz,  $\text{DMSO}-d_6$ ): 31.3 (C- $\omega$ ), 39.5 ( $\text{N}(\text{CH}_3)_2$ ), 55.4 ( $\text{OCH}_3$ ), 56.0 (C- $\delta$ ), 56.4 (C- $\beta$ ), 111.9 (C-9', C-11'), 114.7 (C-9, C-11), 117.1 (C-b'), 120.7 (C-b), 122.4 (C-3', C-5'), 123.3 (C-7'), 123.4 (C-3, C-5), 127.8 (C-7), 130.1 (C-8, C-12), 130.3 (C-8', C-12'), 141.2 (C-a), 142.5 (C-a'), 143.6 (C-2', C-6'), 144.2 (C-2, C-6), 152.0 (C-10'), 153.6 (C-4), 154.0 (C-4'), 161.3 (C-10). Anal. calcd for  $\text{C}_{32}\text{H}_{35}\text{Br}_2\text{N}_3\text{O}$ : C, 56.15; H, 5.15; N, 6.14; found C, 56.25; H, 5.11; N, 6.1. ESI-MS 2 in MeCN,  $m/z$ : calcd 238.8; found 238.9 [2] $^{2+}$ .

### 2.3. Preparation and handling of DNA solutions

Calf thymus DNA (type I; highly polymerized sodium salt, Sigma) was dissolved without further purification in 10 mM sodium phosphate buffer at a concentration of 1–2 mg  $\text{mL}^{-1}$  and kept at 4 °C for at least 16 h. After that the solution was filtered through a PVDF membrane filter (pore size 0.45  $\mu\text{m}$ ) to remove any insoluble material. The concentrations of DNA samples were determined by absorption measurements of the diluted stock solution (1 : 20), using the molar absorption coefficient  $\epsilon_{260} = 12\,824\text{ cm}^{-1}\text{M}^{-1}$  (in base pairs, bp).

### 2.4. Spectroscopic studies

Electronic absorption spectra were recorded on a Varian-Cary 300 spectrophotometer. Fluorescence spectra were recorded on a Cary Eclipse spectrofluorometer. The spectra of circular dichroism were recorded on the automatic recording dichrograph SKD-2MUF. All measurements were carried out in conventional quartz cells of 10 mm path length at 20 °C. The preparation and handling of the solutions were carried out under red light. The experiments were performed in the phosphate buffer solution at pH = 7 or in deionized water. The fluorescence lifetime  $\tau$  was measured in correlated photon counting mode using a Horiba Jobin Yvon Fluorolog 3–221 spectrofluorimeter with 369 and 455 nm nanoleds.

The fluorescence quantum yield measurements were carried out in buffer solutions at  $20 \pm 1$  °C; the concentrations of the studied compounds were  $5 \times 10^{-6}\text{ M}$ . All measured fluorescence spectra were

corrected for the nonuniformity of the detector spectral sensitivity. Coumarin 343 in ethanol ( $\varphi_{\text{fl}} = 0.63$ ) and coumarin 6 ( $\varphi_{\text{fl}} = 0.78$ ) in ethanol was used as a reference for the fluorescence quantum yield measurements. The fluorescence quantum yields were calculated using Eq. (1):

$$\varphi_{\text{fl}}^{\text{fl}} = \varphi_{\text{fl}}^{\text{S}} \cdot \frac{S}{S_{\text{R}}} \cdot \frac{(1 - 10^{-A_{\text{R}}})n^2}{(1 - 10^{-A})n_{\text{R}}^2} \quad (1)$$

wherein  $\varphi_{\text{fl}}^{\text{fl}}$  and  $\varphi_{\text{fl}}^{\text{S}}$  are the fluorescence quantum yields of the studied solution and the standard compound respectively;  $A$  and  $A_{\text{R}}$  are the absorptions of the studied solution and the standard respectively;  $S$  and  $S_{\text{R}}$  are the areas underneath the curves of the fluorescence spectra of the studied solution and the standard respectively; and  $n$  and  $n_{\text{R}}$  are the refraction indices of the solvents for the substance under study and the standard compound.

## 2.5. Molecular modeling calculations

The 3D models of 1a, 1b, 2 and DNA were built using molecular graphics software package Sybyl-X software (Certara, USA). Partial charges on 1a, 1b and 2 atoms were calculated according to the following scheme. First, to find the minimum energy conformation, scanning of the conformational space of the 1a, 1b and 2 was performed with the application of molecular-mechanical approach and Monte-Carlo method by using Molsoft ICM-Pro 3.8.6 [31]. To calculate interatomic interactions the force field MMFF [32] was used at this stage. Further optimization of the conformation found at the first step for the purpose of searching geometry with the smallest energy and calculation of electron density distribution were performed by using second-order Møller-Plesset perturbation theory (MP2) [33] and implicit consideration of the solvent effect with application of the conductor-like polarizable continuum model (CPCM) [34] and cc-pvdz basis sets. Then Merz-Singh-Kollman scheme [35] was applied to obtain electron density distribution for calculation of grid for the electrostatic potential fitting with the following parameters: (6/41 = 10) - the number of surfaces around the atoms and (6/42 = 17) - the density of test points on these surfaces. The RESP (Restrained ElectroStatic Potential) method [36] was applied to fitting of the grid obtained in the previous step for calculation of partial atomic charges. All quantum mechanics simulations were carried out using Gaussian 09 program [37]. To define the most probable binding site of the ligands on the target surface, the procedure of flexible ligand docking was performed using ICM-Pro 3.8.6. DNA conformation remained invariable during the docking procedure. Before starting a docking procedure the structures of DNA and 1a, 1b and 2 were converted into an ICM object according to the ICM method, the molecular models were described using internal coordinates as variables. The parameters needed for interatomic energy calculation and the partial charges for atoms of the targets were taken from the ECEPP/3 [38] and from force field MMFF for atoms of 1a, 1b and 2. The biased probability Monte Carlo (BPMC) minimization procedure [39] was used for global energy optimization. Finally conformational stack obtained from docking procedure was sorted by scoring function. The selected complexes were used as targets during the second docking procedure with subsequent optimization in modeling the possibility of aggregation of the ligands on the surface of the DNA. In the second stage, the complexes, obtained by Molsoft ICM-Pro 3.8.6, were minimized by using SYBYL X and Powell method [40]. The following settings were used: partial charges on the DNA from Amber7 ff02 force field, parameters for interatomic interactions and from Tripos force field [41], a non-bonded cut-off distance equal to 8 Å, a distance-dependent dielectric function, the number of iterations equal to 500, the simplex method in an initial optimization, and an energy gradient convergence criterion of 0.05 kcal/mol/Å.

MD simulations were performed using Amber 18 software [42]. The solvent effect was simulated using the OPC3 water model [43]. The

simulation performed by using periodical boundary conditions and rectangular box. The buffer between DNA-ligand complex and the periodic box wall was at least 15 Å. For neutralizing of the negative charge of DNA backbone  $\text{K}^+$  ions and positive charge of 1a, 1b and 2  $\text{Cl}^-$  were used. The parameters needed for interatomic energy calculation, were taken from the force fields OL15 [44,45] for DNA and from general amber force field (gaff2) for 1a, 1b and 2. At the beginning of the calculation, the systems under study were minimized in two steps. At the first stage, the location of solvent molecules was optimized using 1000 steps (500 steps of the steepest descent, followed by 500 steps of the conjugate gradient), while the mobility of all solute atoms was restrained with a force constant of 500 kcal\* $\text{mol}^{-1}$ \*Å<sup>-2</sup>. At the second stage, the optimization was carried out without any restrictions using 2500 steps (1000 steps of the steepest descent, 1500 steps of the conjugate gradient). Then, gradual heating to 300 K in 20 ps was performed. To avoid too large fluctuations for the systems under study, weak harmonic constraints with a force constant of 10 kcal\* $\text{mol}^{-1}$ \*Å<sup>-2</sup> were used at this stage for all atoms except the solvent atoms. SHAKE algorithm was applied to constrain bonds to hydrogen atoms, that allowed to use 2 fs step. Scaling of nonbonded van der Waals and electrostatic interactions were performed by the standard Amber values. The cut off distance for non-bonded interactions was equal to 10 Å and the long-range electrostatics was calculated using the particle mesh Ewald method. The MD simulations in production phase were carried out using constant temperature ( $T = 300$  K) and constant pressure ( $p = 1$  atm) over 80 ns. To control the temperature Langevin thermostat was used with the collision frequency of 1 ps<sup>-1</sup>. Snapshot visualization was performed using VMD. Energy was estimated using the MM-GBSA approach. The polar contribution  $E_{\text{GB}}$  was computed using the Generalized Born (GB) method and the algorithm developed by Onufriev et al. for calculating the effective Born radii [46]. The non-polar contribution to the solvation energy ( $E_{\text{surf}}$ ), which includes solute-solvent van der Waals interactions and the free energy of cavity formation in solvent, was estimated from a solvent-accessible surface area (SASA). Snapshot visualization was performed using VMD with a donor-acceptor distance of 3.2 Å and angle cut off of 20 degrees. To simulate the interaction of an ensemble of ligands with DNA, the distribution of ligands in the rectangular box was modeled using the PACKMOL package [47] with tolerance distance 10 Å.

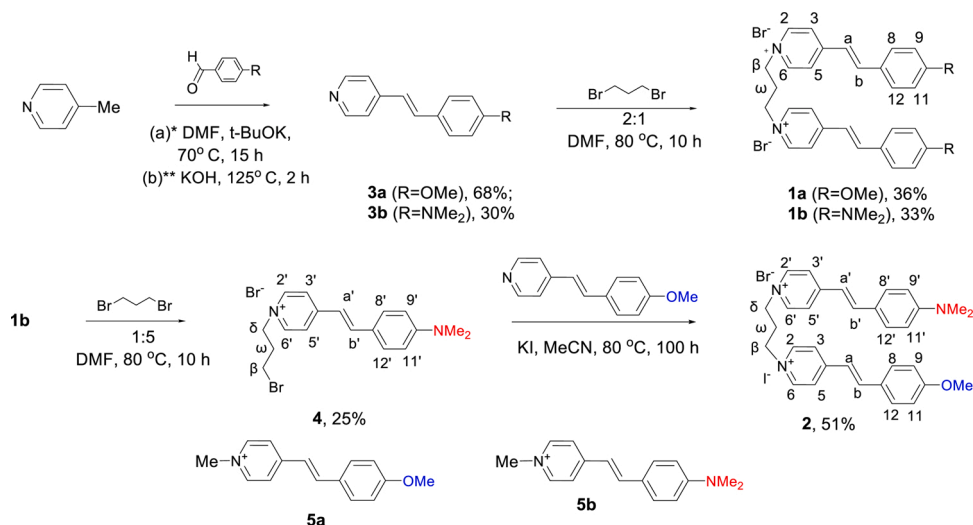
## 3. Results and discussion

### 3.1. Synthesis of bisstyryl dyes 1a, 1b and 2

Symmetric bis(styryl) dyes 1a [48] and 1b [49] were obtained in a two-step synthesis (Scheme 1). In the first step, aldol condensation of 4-picoline with benzaldehyde was performed according to published protocols [28,29] resulting in the mono(styryl) dye 3a and 3b. In the second step, mono(styryl) dyes reacted with 1,3-dibromopropane in ratio 2:1 to give bis(styryl) dyes 1a and 1b. The asymmetric bis(styryl) dye 2 was obtained in 51 % yield by quaternization of the intermediate 4 with 1,3-dibromopropane followed by alkylation of 3b with 1,3-dibromopropane. All dyes 1a, 1b and 2 were identified and fully characterized by NMR spectroscopy, mass spectrometry and elemental analysis (Fig. S1 in Electronic Supporting Information).

### 3.2. Optical properties of dyes 1a, 1b and 2

The absorption spectra in the phosphate buffer (BPE) solution at pH = 7 of symmetric bis(styryl) dyes 1a and 1b exhibit long wavelength absorption bands (LAB) centered at 380 and 468 nm since each of them contains two identical chromophore fragments (Table 1). The positions of LABs are similar to those of corresponding analogue mono(styryl)s 5a and 5b (Table 1). The observed absorption spectra are attributed to an intramolecular charge transfer from the donor OMe or NMe<sub>2</sub> fragment to the acceptor heterocyclic moiety. Absorption spectrum of



**Scheme 1.** Synthesis of the dyes 1a,b and 2 and structures of monostyryl dyes 5a,b [30]. \*Reaction condition for obtaining of 3a. \*\* Reaction condition for obtaining of 3b.

**Table 1**

Optical characteristics of dyes 1a,b, 2, 5a,b and their complexes with DNA ( $\lambda_{\text{abs}}$ ,  $\lambda_{\text{em}}$  - absorption and emission spectral maximum wavelengths;  $I_L$  - fluorescence intensity of free or  $I_{L/DNA}$  - DNA-bound dye at  $\lambda_{\text{em}}$ ;  $\tau$  - fluorescence lifetime at  $\lambda_{\text{em}}$  wavelength).

Dye	$\lambda_{\text{abs}}^{\text{max}}$ , nm		$\lambda_{\text{em}}^{\text{max}}$ , nm		Stoke's shift, $\text{cm}^{-1}$		$I_{L\text{ DNA}}/I_L$ ( $\lambda_{\text{em}}^{\text{max}} L\text{-DNA}$ )	$\phi$ , %		$\tau$ , ns ( $\lambda_{\text{em}}$ , nm) <sup>#</sup>	
	free dye	dye in the presence of DNA	free dye	dye in the presence of DNA	free dye	dye in the presence of DNA		free dye	dye in the presence of DNA	free dye	dye in the presence of DNA ( $C_{\text{dye}}/C_{\text{DNA}} = 1:50$ )
5a	373	395	501	501	6850	5360	2.1	1.2	2.3	< 0.1 (507) 100 %	0.32 (507) 84 % 1.74 (507) 16 %
5b	448	491	615	615	6060	4110	60	0.26	6.2	0.19 (620) 100 %	1.26 (620) 43 % 2.78 (620) 57 %
1a	380	395	510,694	505	6710	5520	3.2	0.47	1.47	< 0.1 (510) 100 %	5.47 (510) 4% 1.57 (660) 100 %
1b	468	492	627	615	5420	4070	60	0.05	2.82	0.21 (520) 100 %	0.42 (620) 63 % 2.57 (620) 37 %
2	401, 503	408, 507	500, 623	495, 615	4940 <sup>a</sup> 3830 <sup>b</sup>	4310 <sup>a</sup> 3460 <sup>b</sup>	3.2, 23	0.04	0.6	0.24 (490) 100 %	0.22 (490) 100 % 0.32 (620) 78 % 2.4 (620) 22 %

<sup>#</sup> - fluorescence decay curves are represented in ESI, Fig. S3.

<sup>a</sup> - Stoke's shift for O-chromophore in bisstyryl dye 2.

<sup>b</sup> - Stoke's shift for N-chromophore in bisstyryl dye 2.

unsymmetrical dye 2 contains two peaks in the long wavelength region at 401 and 503 nm, which are characteristic of both mono(styryl) dyes 5a and 5b. Differences in intensity and some red shift (20–30 nm) in the peak positions on going from equimolar mixture of corresponding mono (styryl)s 5a (O-chromophore), 5b (N-chromophore) can be explained by their intramolecular interaction and the increased polarization of the chromophores and, hence, the more pronounced ICT interaction, resulting from proximity of two positive charges in the structure of 2.

Dyes 1a, 1b and 2 demonstrate large Stoke's shift (5420–6710  $\text{cm}^{-1}$ ). The fluorescence spectrum of dye 1a has a maximum at about 510 nm, corresponding to the O-chromophore 5a, and a maximum at 694 nm. Since the ratio of the intensity of fluorescence signals at 505 nm and 694 nm does not depend on the concentration of 1a in solution, it can be

concluded that the long-wavelength peak corresponds to the excimer fluorescence. Thus, two styryl fragments of dye 1a can form intramolecular face-to-face sandwich H-dimer in aqueous solution (Fig. 1).

The fluorescence decay curves of dyes 5a,b and 1b in water are monoexponential, which indicates the presence of only one type of molecules in the excited state. Time-resolved measurements of 1a showed the existence of short-lived and long-lived components, indicating a relaxation process in the dye molecule with a linear structure and in the form of an intramolecular excimer. When DNA is added to the dyes, the fluorescence decay of the resulting solutions becomes multi-exponential, which indicates that solutions contain two or more components with different fluorescence lifetimes. The average fluorescence lifetime of solutions also increases (Table 1). The large increase in the

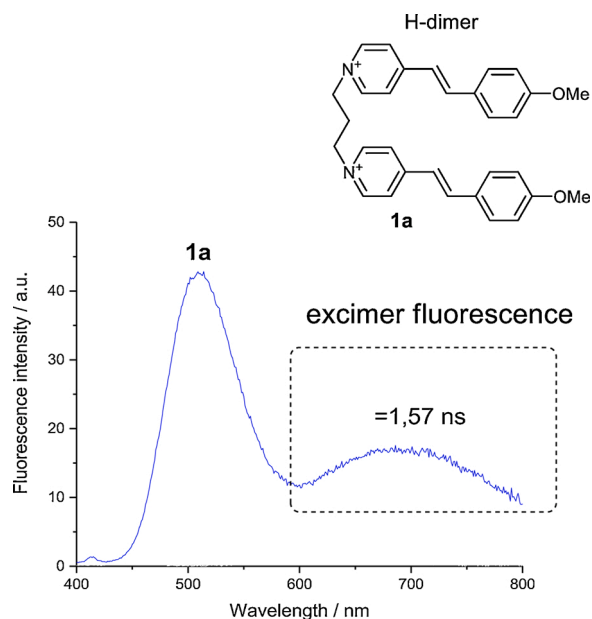


Fig. 1. Fluorescence of 1a at 20°C in BPE buffer and proposed structure of H-dimer.

fluorescence lifetime is primarily due to the fact that interaction with DNA reduces the efficiency of torsional motion of dyes in an excited state around the C=C double bond, making it difficult to form the non-fluorescent Z-isomer. In addition, due to the increased viscosity of samples with a large mass percentage of DNA, the relaxation rate of the excited state of the dye through the formation of the TICT state decreases.

The fluorescence quantum yields of **1b**, **1a** and **2** are very low, obviously due to the presence of efficient competitive nonradiative relaxation processes involving the formation of twisted states and E-Z-isomerization [50]. As shown earlier, the relaxation of the excited state of ligands similar to **1b** goes mainly through the formation of twisted states with a subsequent non-radiative relaxation to the ground state via ‘loose bolt’ mechanism [51]. To support the proposition, the measurements of quantum yields of the fluorescence of dyes **1a**, **b** and **2** in different solvents have been done (Table S1 in ESI). In viscous glycerol and ethylene glycol, an increase in fluorescence quantum yield was observed by 5–6 times for **1a**, 40 times for **1b** and 32 times for **2** due to the suppression of the possibility of rotation around single and double bonds. Also in non-polar solvent the quantum yields of fluorescence are higher than those in polar (Table S1 in ESI). This fact indicates the possibility of the fluorescence enhancement for the dyes under study, when, upon binding to DNA, the dyes pass from water to the hydrophobic environment of the nucleic acid.

The asymmetric dye **2** possesses two different chromophore units between which the occurrence of energy transfer could be. To estimate the possibility and mechanism of it, electrochemical study has been prepared. The redox potentials of dyes **5a**, **5b** and **2** were investigated by cyclic wave voltammetry in MeCN containing tetrabutylammonium hexafluorophosphate as supporting electrolyte on Pt-electrode. The resulting voltammograms, electrochemical data, its analysis and derived HOMO-LUMO energy levels are summarized in ESI (Figs. S6–S8, Table S3.) The mutual arrangement of HOMO-LUMO of **5a** and **5b** is shown in Fig. 2.

As shown in Fig. 2, the LUMOs of the O-chromophore and the N-chromophore of the asymmetric dye **2** are close in energy. They are also located closely on positively charged pyridinium fragments separated only by a short alkyl bridge, which makes possible an electron transfer from an excited chromophore to another one in the ground state. However, the HOMOs of both fragments are localized at the far ends of

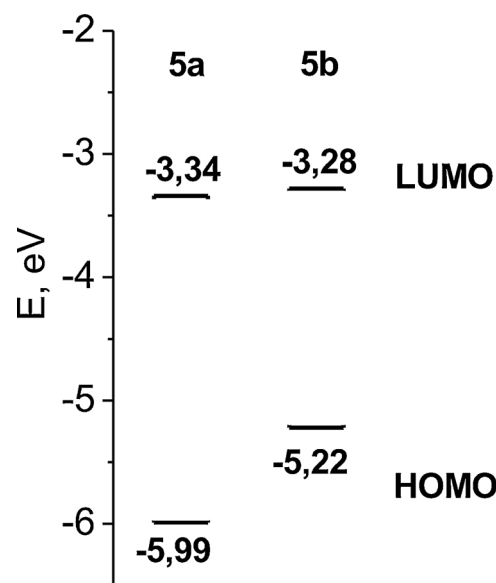


Fig. 2. Mutual arrangement of **5a** and **5b** HOMO-LUMO obtained from electrochemical data.

two chromophores, and the distance between chromophores is 12.3 Å (see Fig. S4 in ESI), which is quite far for Dexter electron transfer [52]. At the same time, the fragments are close enough for FRET (Förster resonance energy transfer), and the HOMO-LUMO gap of **5b** is less than that of **5a**, so FRET from O-chromophore to N-chromophore can occur. The presence and efficiency of FRET was calculated by the optical spectroscopy.

The equimolar mixture of mono(styryl) dyes **5a** and **5b** demonstrates two absorption bands at 382 and 452 nm belonging to O- and N-chromophores (Fig. 3a). Upon excitation the equimolar mixture of **5a** and **5b** with 382 nm light, which is mostly absorbed by O-chromophore **5a**, the emission band at 505 nm is observed similar to that in the spectrum of **5a** (Fig. 3b). The absorption spectrum of **2** recorded under the same conditions is consisted of the same 382 nm and 495 nm bands (Fig. 3c). But irradiation of **2** produces the red-shifted signal at 627 nm belonging to the N-chromophore fluorescence (Fig. 3d). This result indicates occurring of RET from O-chromophore unit to N-chromophore part of **2**. Noteworthy, comparison of the fluorescent spectra of **2** and **5b** presented in Fig. 3b and d shows that the short wavelength part of the emission band of **2** (Fig. 3d) is broadened to some extent by the residual fluorescence of the donor unit. Using the emission intensities at 500 nm where the acceptor chromophore does not emit light (see Fig. 3b) for compound **2** (*I*) and equimolar mixture of **5a** and **5b** (*I*<sub>0</sub>), the energy transfer efficiency was calculated to be as high as 0.97 (97 %) according to the equation:

$$\Phi_{\text{RET}} = 1 - \frac{I}{I_0}$$

A rather close value of  $\Phi_{\text{RET}}$  (99 %) was obtained using the theoretical calculations by the Förster model. Theoretical calculation of  $\Phi_{\text{RET}}$  is presented in part 3, Figs. S4, S5 and Table S2 in ESI.

### 3.3. Study of the interaction of 1a, b and 2 with ct-DNA by optical methods

The interaction of bis(styryl) dyes **1a**, **b** and **2** with calf thymus DNA was investigated by spectrophotometric and spectrofluorimetric titrations in BPE buffer at pH = 7. The changes in optical spectra were analyzed by varying concentrations of DNA in the presence of a constant concentration of each dye. For all dyes two processes have been observed. Initially the addition of DNA to the solution of bis(styryl) dyes

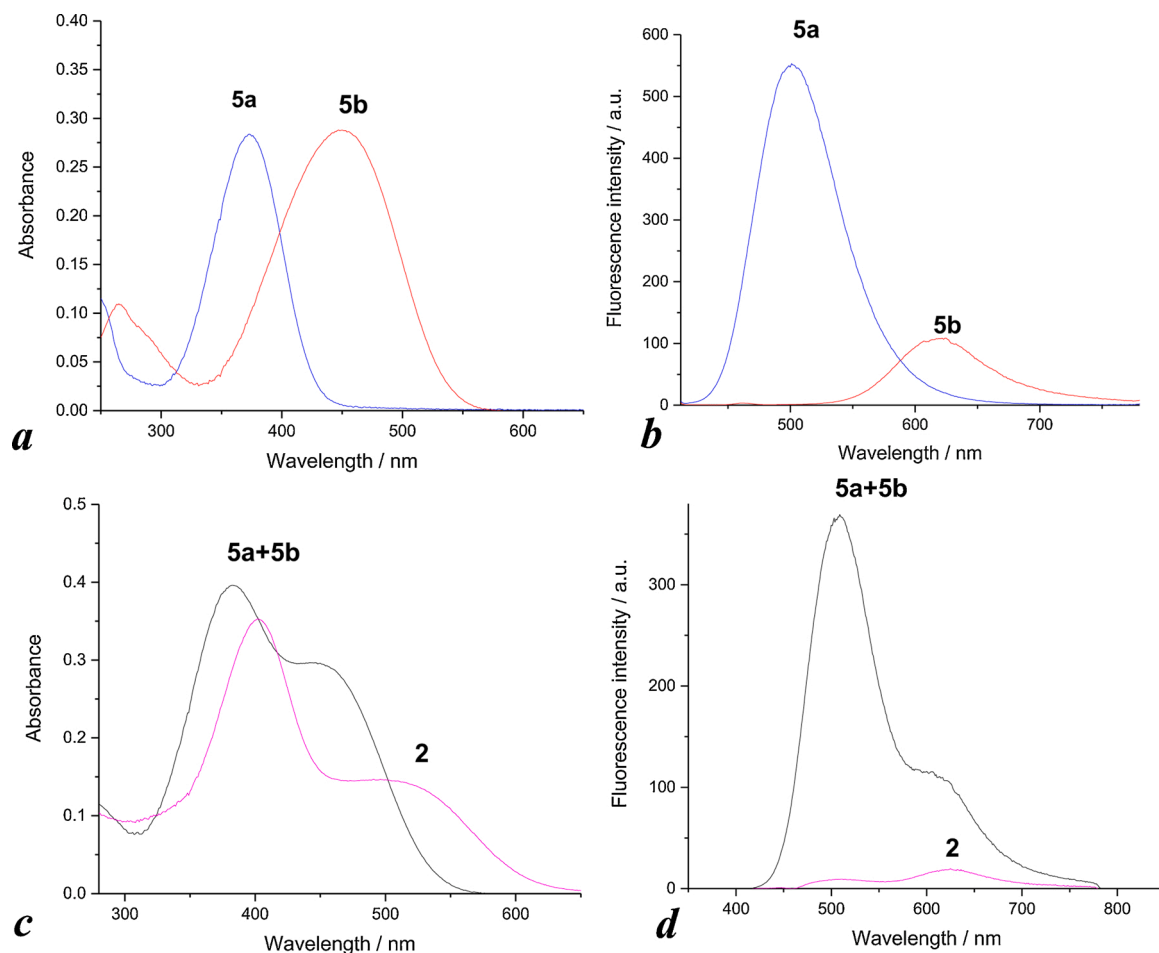


**Fig. 3.** Absorption (a,c) and fluorescence (b,d) spectra of compounds **2** (c,d), **5a** (a,b), **5b** (a,b) and equimolar mixture of **5a** and **5b** (c,d) in BPE buffer. Concentrations of all compounds were 10  $\mu$ M. Excitation wavelengths  $\lambda_{ex}$  were 450 nm for **5b** and 382 nm for **2**, **5a** and mixture of **5a** and **5b**.

**1a**, **b** and **2** causes a decrease in the intensity of the absorption band with a small red shift of the absorption maximum (Fig. 4a–c). The further increase in DNA concentration leads to a rise of the intensity of the absorption band and its bathochromic shift up to 15 nm for **1a** and 24 nm for **1b** (Fig. 4a and b). The addition of DNA to the solution of bis(styryl) dye **2** showed smaller changes in position of bands and intensity of absorption. Here the DNA induced spectral changes may be explained in terms of change in local polarity around the dye. The polarity of the environment around the dye decreases with the addition of DNA, and the energy gap between the highest occupied molecular orbital (HOMO) and the lowest unoccupied molecular orbital (LUMO) of the dye decreases, which is reflected as bathochromic shift [53].

The interaction of monostyryl dyes **5a**, **b** with DNA also demonstrates the bathochromic shift of the long wavelength band in absorption spectra (Figs S9 and S10 in ESI). The binding constants ( $K_b$ ) and the number of dsDNA base pairs occupied by one bound dye molecule ( $n$ ) for the dyes **5a**, **b** were estimated by spectroscopic titrations. The approximation of the experimental results with the McGhee and von Hippel equation shows that  $K_b$  values obtained for the dyes **5a** and **5b** were  $4.9 \times 10^3 \text{ M}^{-1}$  and  $3.2 \times 10^3 \text{ M}^{-1}$  respectively, the number of dsDNA base pairs occupied by one bound dye molecule ( $n$ ) were correspondingly 3.74 and 3.80 [54].

The fluorimetric response of the dyes to the association with DNA is even more complicated (Fig. 5). For the bis(styryl) dye **1a**, the position

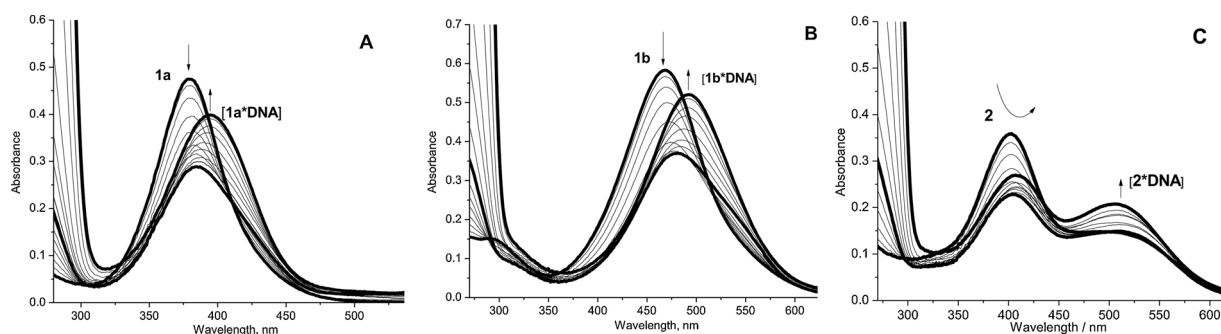


**Fig. 4.** Photometric titration of ct-DNA to bis-styryl dyes **1a**,  $c_{DNA}/c_{1a} = 0-49$  (a); **1b**,  $c_{DNA}/c_{1b} = 0-44$  (b); **2**,  $c_{DNA}/c_2 = 0-42$  (c);  $c_{lig} = 10 \mu\text{M}$ ; in BPE buffer. The arrows show the change in the intensity of the absorption bands upon the addition of ct-DNA.

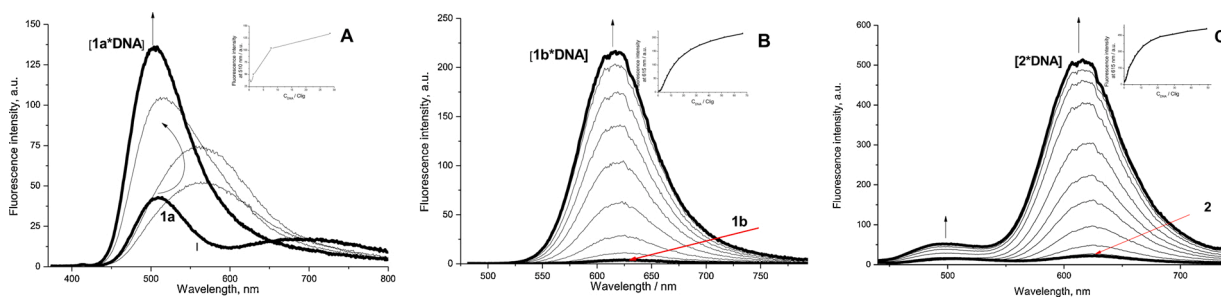


**Fig. 5.** Fluorimetric titration of ct-DNA to bis-styryl dyes **1a**,  $c_{\text{DNA}}/c_{1a} = 0\text{--}29$  (a); **1b**,  $c_{\text{DNA}}/c_{1b} = 0\text{--}67$  (b); **2**,  $c_{\text{DNA}}/c_2 = 0\text{--}48$  (c);  $c_{\text{lig}} = 10 \mu\text{M}$ ; in BPE buffer. The arrows show the change in the intensity of the emission bands upon the addition of ct-DNA.

of the fluorescence maximum change after the addition of the first aliquots of DNA ( $c_{\text{DNA}}/c_{1a} = 0.75$  and  $1.63$ ), while the intensity increased slightly. In this case, the destruction of the intramolecular excimer can be observed, apparently when adding DNA to the dye, interaction with ds-DNA becomes more beneficial. With the increasing concentrations of DNA ( $c_{\text{DNA}}/c_{1a} = 29$ ), the emission intensity of **1a** significantly increased with a 5 nm blue shift of the maximum (Fig. 5a). The first additions of DNA to a solution of bis(styryl) **1b** did not in any way affect the change in the dye fluorescence signal, but with a further increase in the DNA concentration ( $c_{\text{DNA}}/c_{1b} = 67$ ), the intensity increased up to 60 times (Fig. 5b). For the dye **2**, the first additions of DNA increased the intensity of the far-wave fluorescence band, while the band at 500 nm remained practically unchanged. Further, there was an intense increase in fluorescence at 620 nm and a slight increase in the intensity of the short-wavelength band (Fig. 5c). Such changes confirm the presence of energy transfer in the molecule, therefore the binding of each of the chromophores led to an increase in the fluorescence intensity of the N-chromophore at 620 nm. Similar to what we saw when dyes **1a**, **b** and **2** demonstrated the enhancement of fluorescence in viscous solvent, the fluorescence of dyes increased when they placed in the DNA solution. The restricted motional freedom for rotation around single and double bond results in styryl energy dissipation predominantly throughout emission via fluorescence. Analogue to glycerol solution, the most pronounced enhancement was found for **1b** and **2** (Table 1).

### 3.4. Study of the interaction of **1a**, **1b** and **2** with ct-DNA by CD spectroscopy

For a better understanding the structure of dye-ds-DNA complexes, we used CD spectroscopy as a highly sensitive method for detecting conformational changes in the secondary structures of nucleic acid [55]. Dye molecules **1a**, **b** and **2** are achiral and do not give a signal in the CD spectra. Small achiral molecules can acquire an induced CD spectrum when bound to nucleic acid (usually analyzed in the  $> 300$  nm range), which can be useful for determining binding modes (intercalation, association, groove binding, etc.) [56]. Fig. 6a–e show the DNA-induced CD spectra of dyes **5a**, **b**, **1a**, **b** and **2**. Minor groove binding of **5a** and **5b** to ds-DNA gives a low-intensive positive ICD band (Fig. 6a, b). In the ICD spectrum of dye **1a** the appearance of a strong exciton CD signal is observed (Fig. 6c). The exciton CD signal has a one positive and one negative bands on either sides of the absorption maximum of the free ligand [57,58]. Excitonic CD indicates the formation of dimers or higher order complexes, either in the groove-binding mode or in the external stacking-binding mode [56,59,60]. It is possible to propose the formation of a structure in which two dyes form a cofacial dimer within the minor groove of DNA and adjacent dimers fill the minor groove along the length of the DNA. The interaction between adjacent dimers in the minor groove causes the splitting of the band into positive and negative peaks [61]. The right-handed helical orientation of adjacent dimers results in order of the bands when positive is at long wavelength and negative is at short wavelength. In the case of compounds **1a**, the

isoelliptic points coincide with the zero transition and are centered at the wavelengths corresponding to the absorption maximum of the dye (**1a**: 380 nm). This phenomenon is known as right-handed helical aggregation in DNA template [62]. As the concentration of DNA increases, the dimers begin to spread out along the groove. In CD spectra the rise in DNA concentration leads to the splitting is lost (Fig. 6b–d).

The binding of a single molecule in the minor groove is favorable based on the hydrophobicity of the dye. If a second dye enters the groove to form a dimer, then the dyes will have more favorable van der Waals interactions with each other. The assembly of one dimer widens the minor groove, what do ease the assembly of additional dimers due to the groove would already be pre-organized. The second level of cooperativity is the assembly of end-to-end aggregates in the minor groove at high dye concentrations. While distorting the DNA should diminish the face-to-face cooperativity, the van der Waals dye interactions are sufficiently strong to compensate for this [2].

Since we did not detect the formation of dimers or aggregates in a solution of the free dye **1b**, and the cleavage of the CD signal indicates the formation of aggregates in the DNA groove it can be assumed that aggregates are formed already in the DNA body.

Upon the binding of **1b**, the DNA helix preserves its right-handed arrangement, whereas the exciton splitting of the dye ICD indicates the formation of the left-handed helical assembly of the aggregating chromophores [26]. For bisstyryl **1b** the isoelliptic points appear at 476 and 537 nm, i.e. one is significantly red-shifted in comparison with the absorption maximum of free **1b** ( $\Delta\lambda = +69$  nm) that may be indicative of the formation of J-type dimers in the DNA groove.

In the case of compound **2**, the isoelliptic points appear at 439 nm and 477 nm, i.e. it is shifted in comparison with the absorption maximum of free **2** ( $\Delta\lambda_1 = +38$  nm,  $\Delta\lambda_2 = -26$  nm). The extent of aggregation is not very high because of the relatively low intensity of the CD exciton coupled band that arises from side interactions when the dimers in the groove have tight contact with each other. Such changes in the CD spectra may indicate that bis(styryl) dye molecules interact with DNA by folding into the groove.

### 3.5. Competitive displacement assay by bisstyryl dyes **1a**, **1b** and **2**

The DNA-binding mode of bis(styryl) dyes **1a**, **1b** and **2** was further investigated using a dye displacement assay which is simply based on the principle that if a small molecule or bis(styryl) replaces the DNA-bound dye, this indicates that the molecule binds to DNA in a similar way. Substitution of a dye for a small molecule results in changes in fluorescence intensity which can be easily identified by changes in the fluorescence spectra.

To this end, we first studied the dye displacement assay using MeGr (methylene green), ligand for DNA major groove [63]. As shown in Fig. S11a–c in ESI, subsequent addition of bis(styryl) dyes **1a**, **1b** or **2** had no effect on MeGr-ct-DNA complex, indicating that bis(styryl)s do not follow major groove binding mode.

To further investigate the groove-binding mode of binding we

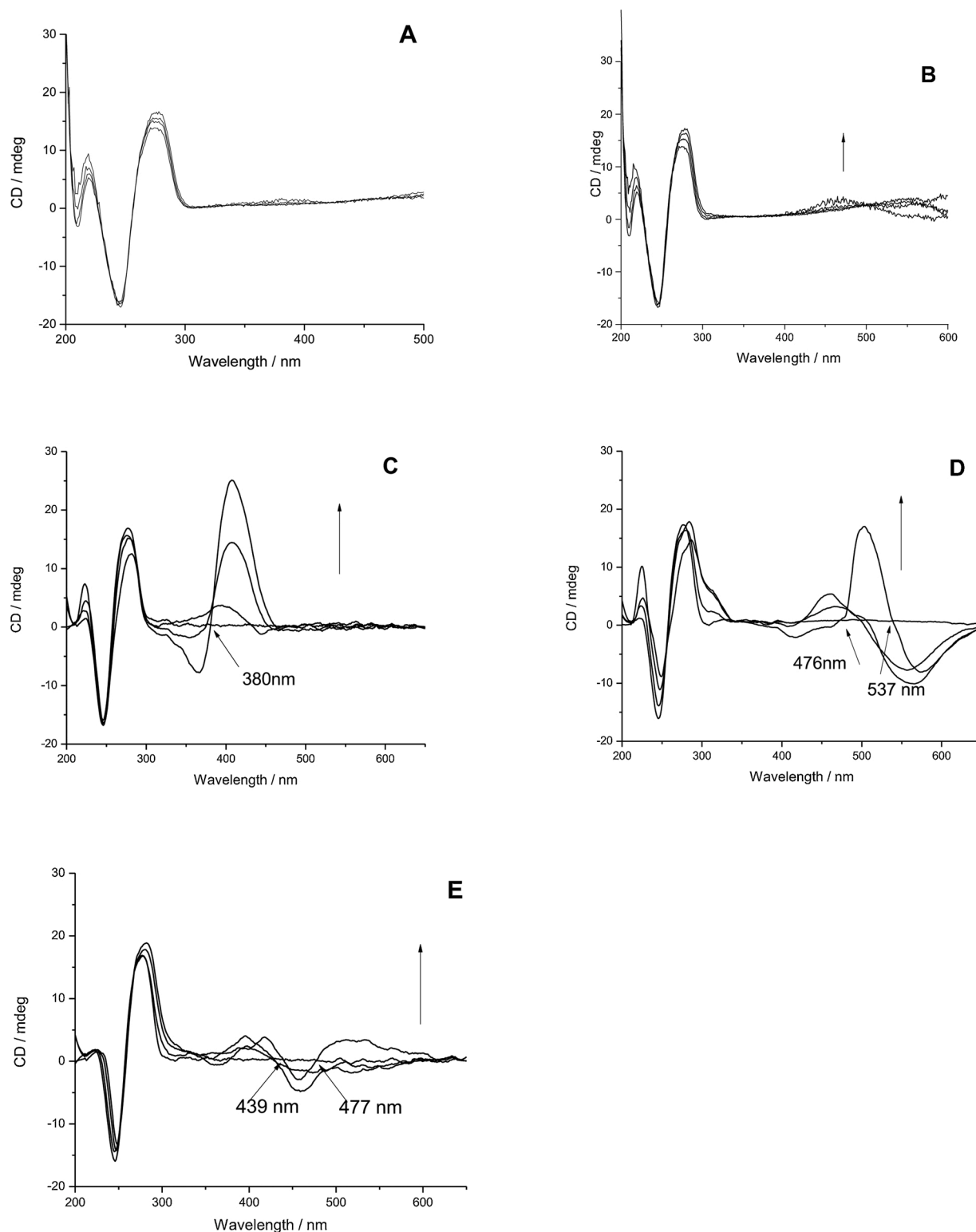


**Fig. 6.** Circular dichroism spectra of ct-DNA (cDNA = 0.1 mM b.p.) in the absence and presence of bis-styryl dyes 5a(a), 5b(b), 1a(c), 1b(d) and 2(e) at different LDRs (ligand–DNA ratio): 0; 0.1; 0.3; 0.6. 5a, 5b, 1a, 1b, 2: in BPE buffer. The arrows show the changes in the bands with increasing dye concentration.

studied the displacement of the Hoechst 33258 dye, minor groove binding dye [64]. The groove-binding molecules are able to displace Hoechst 33258 from the minor groove of DNA helix, which leads to decrease fluorescence intensity of the DNA-Hoechst system. As shown in Figs. 7 and S12 in ESI, subsequent addition of dyes 1a, 1b or 2 to the Hoechst-ct-DNA complex led to successive decrease in fluorescence maxima intensity suggestive of minor groove binding mode of bis(styryl)

s.

### 3.6. Molecular modeling calculations of binding of bisstyryl dyes 1a, 1b and 2 with DNA

In order to determine the probable conformation of compounds 1a, 1b, and 2 in solution, quantum-mechanical optimization was carried out

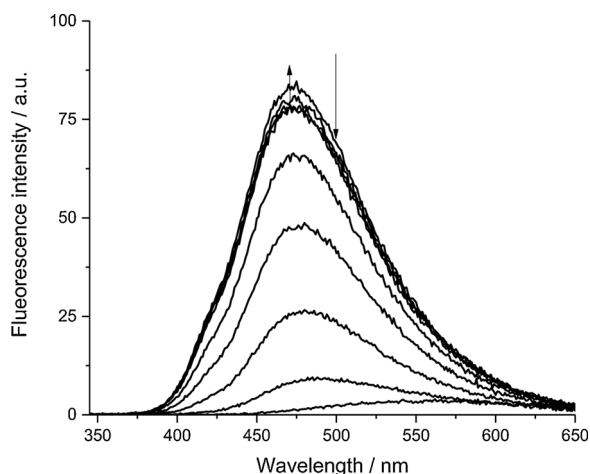


Fig. 7. Fluorimetric titration of complex Hoechst-ct-DNA by bis(styryl) dyes 1a,  $C_{1a}/C_{\text{Hoechst}} = 0-12$ ;  $C_{\text{Hoechst}} = 5 \mu\text{M}$ ;  $C_{\text{DNA}} = 0.15 \text{ mM}$  in BPE buffer. The arrows show the change in the intensity of the emission bands upon the addition of ct-DNA.

using the second-order Møller-Plesset procedure and implicitly taking into account the effect of the solvent in the framework of the conductor-like polarizable continuum model. The results of quantum mechanical simulation are shown in Fig. 8.

The results obtained in Fig. 8 indicate the possibility of the formation of an intramolecular sandwich structure for all three molecules of bis-styryl dyes in solution. The most stringent parallel arrangement of styryl fragments is observed in the case of 1a; in the remaining molecules, styryl fragments are displaced relative to each other. This is consistent with the experimental fact that registration of excimer fluorescence is observed only in the case of compound 1a. Molecular modeling also showed the transition of dyes from a sandwich structure to a linear structure as a result of thermal fluctuations. Future calculation analysis of the bisstyryl dyes organization in solution is presented in ESI, part 7, Figs S13, S14.

Modeling of compounds 1a, 1b and 2 with DNA was carried out in two stages. The sequence 5'-AACCGGTTACGTACGT-3' was used to build a DNA model. First, a docking procedure was carried out in order to establish the probable geometry of the dye on the DNA surface.

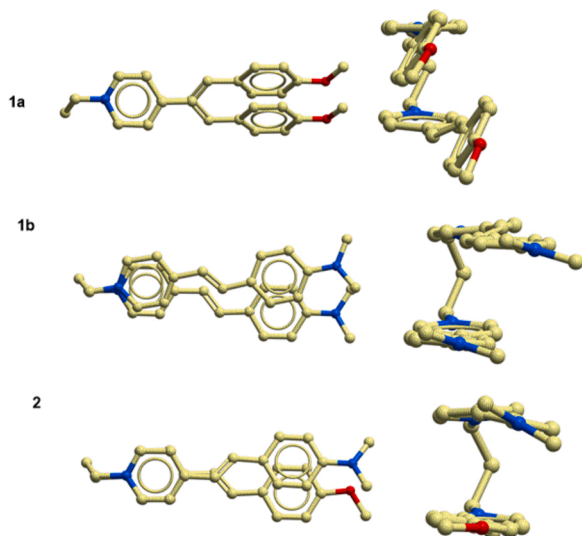


Fig. 8. Conformations of 1a, 1b and 2 obtained as a result of quantum mechanical optimization. Atoms are colored as follows: carbons - yellow, nitrogen - blue, oxygen - red. Hydrogen is not shown.

Fig. S15 in ESI shows the docking results. When interacting with DNA, all compounds are located in a minor groove; the most probable conformation is one in which the styryl fragments are in linear forms.

The docking procedure implicitly evaluates the effect of a solvent on the mechanism of interaction with DNA; therefore, at the second stage of calculations, to refine its results, we performed modeling using molecular dynamics and adding interactions with solvent molecules to the calculations. In the calculations, the starting conformations for all compounds were taken in the form of both sandwich and open linear structures. The starting conformations were localized at a distance that almost excluded the interaction of ligands in the target. Analysis of the simulation data showed that in the first close contact with the DNA surface in all three cases occurred due to the convergence of the positively charged pyridine rings. During the interaction of 1a in the form of a sandwich with DNA, it was observed to fold into a minor groove, as well as the initial transition of the molecule into a linear form and subsequent interaction with DNA. In cases 1b and 2, the conformation in the form of a sandwich was retained when folded into the minor groove. Fig. 9 shows the starting and obtained at the last step trajectories of the conformation of DNA complexes with 1a, 1b, and 2, when the initial conformation of the bisstyryl dye had a sandwich structure. Fig. 10 shows the process of interaction with DNA of linear dyes.

According to the data shown in Fig. S17 in ESI, the free energy of the dye in the sandwich form is lower than those of linear form. This is explained by that the mutual arrangement of styryl fragments in the sandwich leads to a twofold increase in the interacting pairs and the appearance of  $\pi-\pi$  interactions between pyridine and benzene rings. The analysis of the change in the binding energy of the dye with DNA with time obtained in the performed calculations is shown in Fig. S16 in ESI. From the data obtained, it can be concluded that the interaction energy of 1a, 1b and 2 in the linear form with DNA is 10–15 kcal/mol lower, even taking into account the fact that the transition from the sandwich form to the linear one requires an energy of 8–10 kcal/mol. This is due to the fact that, in the case of a sandwich, the area of contact with the DNA surface is two times less, which leads to a significant decrease in the Coulomb and Van der Waals interactions and the nonpolar component of the solvation energy.

To analyze the formation of aggregates in the minor groove of DNA, calculations of the DNA complex formed in the presence of 50 molecules 1a and 1b were performed. Modeling for dye 2 was not performed, since, according to experimental data, the aggregation process for this dye is insignificant. The structure of aggregates in the groove of DNA formed from dyes in a sandwich form is shown in Fig. 9. For compound 1a, the most probable arrangement of molecules is along a narrow groove in such a way that the pyridine site of one sandwich is adjacent to the aryl fragment of the other. Aggregates formed from 1b fit into a minor groove perpendicular to the DNA surface (Fig. 9). This type of molecular packing provides a tighter packing and, consequently, a stronger hydrophobic interaction of molecules with the DNA groove.

Fig. 10 shows the calculated structures of dimeric aggregates formed from dyes 1a and 1b in the minor groove of DNA. Fig. S18 in ESI presents graphs characterizing the change in the mutual arrangement of styryl dyes 1a and 1b in dimeric aggregates. As parameters, we used the distance between the centers of mass of the pyridine and benzene fragments, and the angle between the vectors connecting the centers of mass of the pyridine and benzene fragments related to the molecules located one above the other. An analysis of the parameter values shows that the arrangement of the styryl fragments of two molecules one above the other is stable. The overlap occurs at an acute angle, the value of which in case 1b is less than in case 1a. The shift of the styryl fragment relative to the other along the minor groove is more pronounced in case 1a.

#### 4. Conclusion

The investigation of mechanism of the bis(styryl) dye – ct-DNA interaction has been done applying of three different bis(styryl)

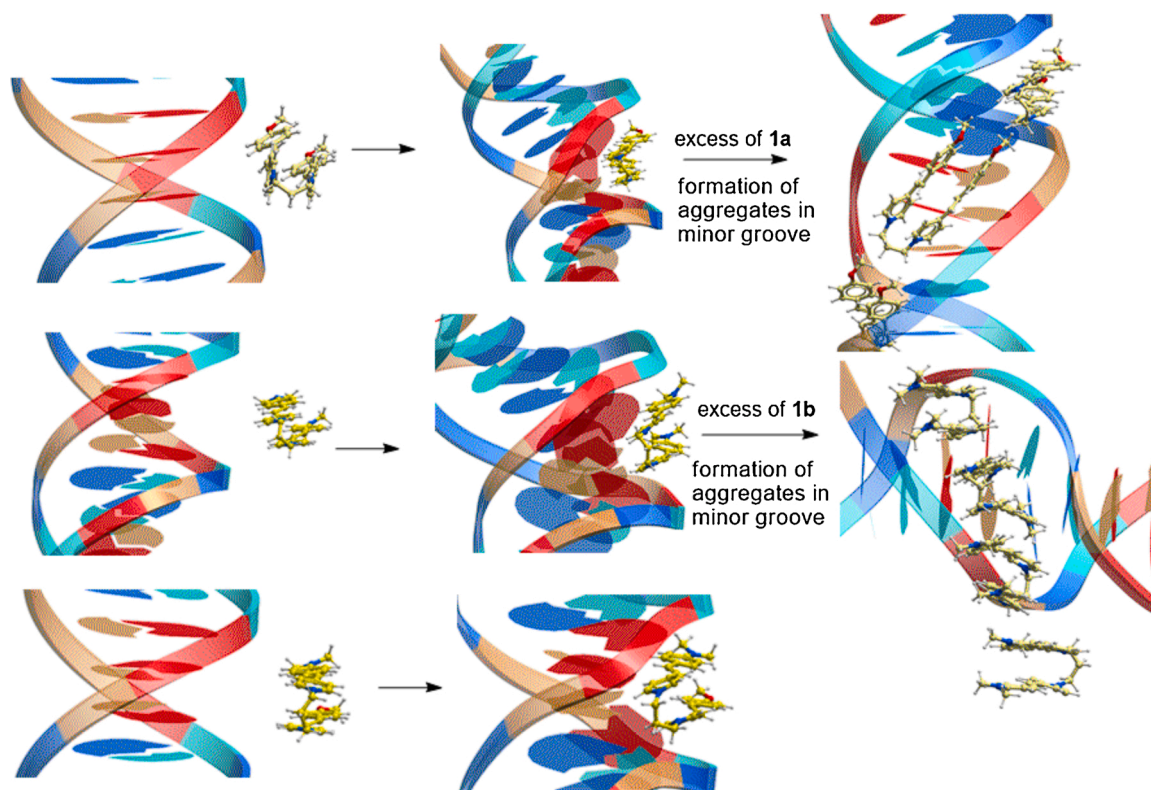


Fig. 9. Conformations, starting and obtained at the last step of MD calculations, of complexes DNA with 1a, 1b and 2 (initial dyes in sandwich form).

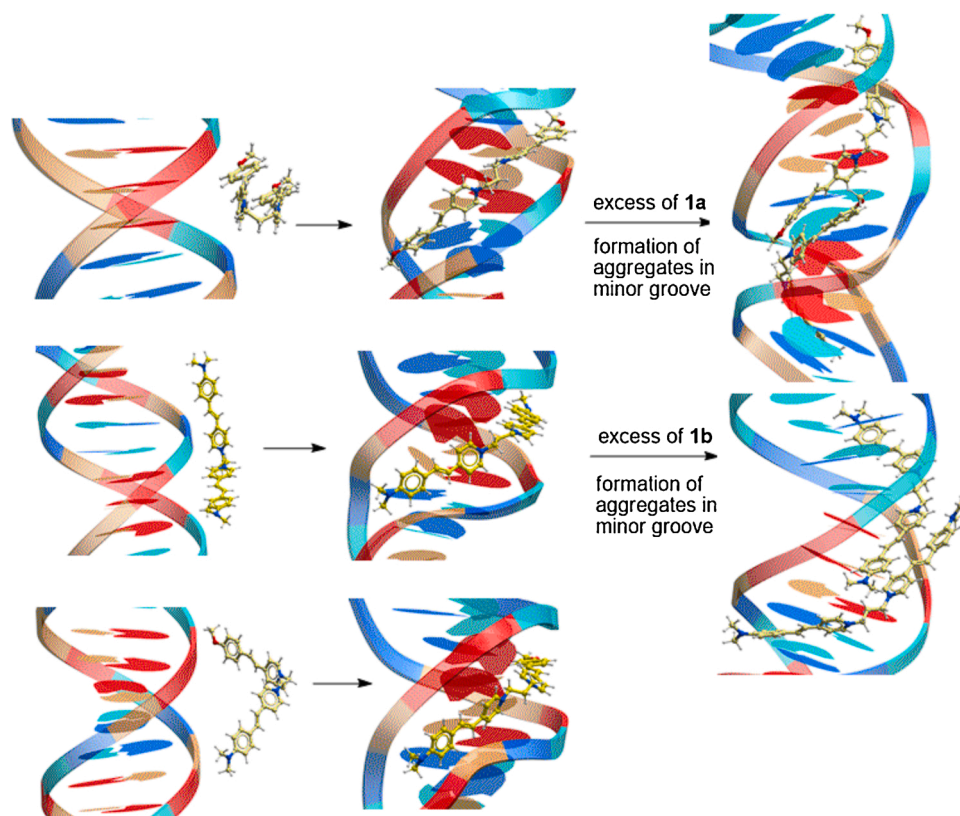


Fig. 10. Conformations, starting and obtained at the last step of MD calculations, of complexes DNA with 1a, 1b and 2 (initial dyes 1b and 2 in linear form, dye 1a as H-dimer).

pyridinium dyes possessing OMe or/and NMe<sub>2</sub> substituents in phenyl ring by using of UV-vis and fluorescence spectroscopic techniques, circular dichroism (CD), Hoechst 33258 displacement experiments and quantum-chemical calculations. According to MD calculations the initial dyes can exist in water solution in linear and intramolecular sandwich forms. The interaction with DNA can occur with both forms of dyes. For all studied dyes the two step interaction with DNA has been found. At high dye concentration the binding of a pair of dyes in the minor groove forces the groove to widen, making it energetically favorable for a second pair of dyes to bind adjacent to the first dimer along the long axis of the minor groove. According to the MD calculations the formation of aggregates can occur from the dyes as in sandwich H-dimer as well as linear forms. The formation of dye aggregates was confirmed by experimental methods, but the obtained experimental data do not allow making an unambiguous conclusion about what type of aggregation (“folded” or “extended”) is observed for the dyes under study. Cooperative assembly of multiple dyes in DNA minor groove results in the formation of helical dye aggregates that exhibit large circular dichroism (CD) signals. In case of bis(styryl) dye 1a containing OMe substituent in phenyl ring, the obtained results indicate the formation of aggregates of right-handed chirality. For bis(styryl) dye 1b the left-handed helical assembly of the aggregating chromophores was revealed. We assumed that the difference in aggregate chirality could be due to the fact that formation of 1a aggregates occurs from “extended” dye form, whereas, dye 1b forms the aggregates in “sandwich” form. Dye 2 composed from OMe- and NMe<sub>2</sub>-containing chromophores is able to form the aggregates in less extend if compare with dyes 1a and 1b. The formation of aggregates in solution or in the body of DNA has not been found for monostyryl dyes 5a, 5b. This is consistent with the lack of literature data on the formation of aggregates of monostyryl dyes in the presence of DNA.

The fluorescence response upon binding of dyes to DNA strongly depends on the nature of the substituents in the dye molecules. Thus, dyes 1b, 2 and 5b containing NMe<sub>2</sub> substituents demonstrate an increase in fluorescence quantum yield up to 56 times upon binding to DNA. Whereas for dyes 1a and 5a containing OMe groups, the increase in the fluorescence quantum yield upon binding to DNA does not exceed 3.1 times.

In free and bound with DNA dye 2 the effective resonance energy transfer was proved between OMe- and NMe<sub>2</sub>-containing chromophores. Such chromophoric pair provides the system with large Stoke’s shift. It absorbs at 408 nm and emits at 615 nm.

The study of bis(styryl) dye-DNA interaction reveals what structural fragments in composition of dye provides the desirable mode of complex, the investigation could be very important for designing an improved imaging and therapeutic agents.

## Statement

**Maria A. Ustimova:** Investigation, Validate, Visualization, Writing-Original draft preparation. **Yury V. Fedorov:** Methodology, Formal analysis, Writing- Reviewing and Editing. **Vladimir B. Tsvetkov:** Investigation, Methodology, Formal analysis, Validate, Writing- Original draft, Visualization. **Sergey D. Tokarev:** Investigation, Validate. **Nikolai A. Shepel:** Investigation. **Olga A. Fedorova:** Methodology, Formal analysis, Conceptualization, Writing- Original draft preparation, Writing- Reviewing and Editing.

## Declaration of Competing Interest

The authors declare that they have no known competing financial interests or personal relationships that could have appeared to influence the work reported in this paper.

## Acknowledgments

Financial support from the Russian Foundation for Basic Research project N<sup>o</sup> 19-03-00535 (synthesis and optical studies), Russian Scientific Foundation N<sup>o</sup> 19-73-20187 (CD spectroscopy studies and MD calculations) and equipment facilities from Center of collective facilities of A.N. Nesmeyanov Institute of Organoelement compounds of Russian Ministry of Sciences and High Education are gratefully acknowledged.

## Appendix A. Supplementary data

Supplementary material related to this article can be found, in the online version, at doi:<https://doi.org/10.1016/j.jphotochem.2021.113378>.

## References

- [1] S. Mukamel, D.S. Chemla, Preface, *Chem. Phys.* 210 (1996) vii–viii, [https://doi.org/10.1016/s0301-0104\(96\)90047-6](https://doi.org/10.1016/s0301-0104(96)90047-6).
- [2] A. Pawlik, S. Kirstein, U. De Rossi, S. Daehne, Structural conditions for spontaneous generation of optical activity in J-aggregates, *J. Phys. Chem. B* 101 (1997) 5646–5651, <https://doi.org/10.1021/jp9708308>.
- [3] A. Kurutos, O. Ryzhova, V. Trusova, U. Tarabara, G. Gorbenko, N. Gadjev, T. Deligeorgiev, Novel asymmetric monomethine cyanine dyes derived from sulfobetaine benzothiazolium moiety as potential fluorescent dyes for non-covalent labeling of DNA, *Dyes Pigm.* 130 (2016) 122–128, <https://doi.org/10.1016/j.dyepig.2016.03.021>.
- [4] H. Hilal, J.A. Taylor, Cyanine dyes for the detection of double stranded DNA, *J. Biochem. Biophys. Methods* 70 (2008) 1104–1108, <https://doi.org/10.1016/j.jprot.2007.12.008>.
- [5] T.Y. Ogul'chansky, M.Y. Losytskyy, V.B. Kovalska, V.M. Yashchuk, S.M. Yarmoluk, Interactions of cyanine dyes with nucleic acids. XXIV. Aggregation of monomethine cyanine dyes in presence of DNA and its manifestation in absorption and fluorescence spectra, *Spectrochim. Acta - Part A Mol. Biomol. Spectrosc.* 57 (2001) 1525–1532, [https://doi.org/10.1016/S1386-1425\(01\)00437-1](https://doi.org/10.1016/S1386-1425(01)00437-1).
- [6] B.A. Armitage, Cyanine dye-DNA interactions: intercalation, groove binding, and aggregation, *Top. Curr. Chem.* 253 (2005) 55–76, <https://doi.org/10.1007/b100442>.
- [7] A.L. Mikheikin, A.L. Zhuze, A.S. Zasedatelev, Binding of symmetrical cyanine dyes into the DNA minor groove, *J. Biomol. Struct. Dyn.* 18 (2000) 59–72, <https://doi.org/10.1080/07391102.2000.10506647>.
- [8] R. Cao, C.F. Venezia, B.A. Armitage, Investigation of DNA binding modes for a symmetrical cyanine dye trication: effect of DNA sequence and structure, *J. Biomol. Struct. Dyn.* 18 (2001) 844–856, <https://doi.org/10.1080/07391102.2001.10506712>.
- [9] H.J. Karlsson, P. Lincoln, G. Westman, Synthesis and DNA binding studies of a new asymmetric cyanine dye binding in the minor groove of [poly(dA-dT)]<sub>2</sub>, *Bioorg. Med. Chem. Lett.* 11 (2003) 1035–1040, [https://doi.org/10.1016/S0968-0896\(02\)00463-7](https://doi.org/10.1016/S0968-0896(02)00463-7).
- [10] H.J. Karlsson, M. Eriksson, E. Perzon, B. Åkerman, P. Lincoln, G. Westman, Groove-binding unsymmetrical cyanine dyes for staining of DNA: syntheses and characterization of the DNA-binding, *Nucleic Acids Res.* 31 (2003) 6227–6234, <https://doi.org/10.1093/nar/gkg821>.
- [11] J.G. Pelton, D.E. Wemmer, Structural modeling of the distamycin A-d(CGCGAATTCGCG)<sub>2</sub> complex using 2D NMR and molecular mechanics, *Biochemistry* 27 (1988) 8088–8096, <https://doi.org/10.1021/bi00421a018>.
- [12] J.G. Pelton, D.E. Wemmer, Structural characterization of a 2:1 distamycin A · d(CGCAAATTCGCG) complex by two-dimensional NMR, *Proc. Natl. Acad. Sci. U. S. A.* 86 (1989) 5723–5727, <https://doi.org/10.1073/pnas.86.15.5723>.
- [13] X. Chen, B. Ramakrishnan, S.T. Rao, M. Sundaralingam, Binding of two distamycin A molecules in the minor groove of an alternating b-DNA duplex, *Nat. Struct. Biol.* 1 (1994) 169–175, <https://doi.org/10.1038/nsb0394-169>.
- [14] X. Chen, B. Ramakrishnan, M. Sundaralingam, Crystal structures of the side-by-side binding of distamycin to AT-containing DNA octamers d(ICITATIC) and d(ICATATIC), *J. Mol. Biol.* 267 (1997) 1157–1170, <https://doi.org/10.1006/jmbi.1997.0941>.
- [15] D. Suh, J.B. Chaires, Criteria for the mode of binding of DNA binding agents, *Bioorg. Med. Chem. Lett.* 3 (1995) 723–728, [https://doi.org/10.1016/0968-0896\(95\)00053-J](https://doi.org/10.1016/0968-0896(95)00053-J).
- [16] M.Q. Wang, S. Liu, C.P. Tang, A. Raza, S. Li, L.X. Gao, J. Sun, S.P. Guo, Flexible amine-functionalized triphenylamine derivative as a fluorescent “light-up” probe for G-quadruplex DNA, *Dyes Pigm.* 136 (2017) 78–84, <https://doi.org/10.1016/j.dyepig.2016.08.041>.
- [17] A.O. Balanda, K.D. Volkova, V.B. Kovalska, M.Y. Losytskyy, V.P. Tokar, V. M. Prokopets, S.M. Yarmoluk, Synthesis and spectral-luminescent studies of novel 4-oxo-4,6,7,8-tetrahydropyrrolo[1,2-a]thieno[2,3-d]pyrimidinium styryls as fluorescent dyes for biomolecules detection, *Dyes Pigm.* 75 (2007) 25–31, <https://doi.org/10.1016/j.dyepig.2006.05.010>.
- [18] V.B. Kovalska, M.Y. Losytskyy, D.V. Kryvorotenko, A.O. Balanda, V.P. Tokar, S. M. Yarmoluk, Synthesis of novel fluorescent styryl dyes based on the imidazo[1,2-a]pyridinium chromophore and their spectral-fluorescent properties in the

- presence of nucleic acids and proteins, *Dyes Pigm.* 68 (2006) 39–45, <https://doi.org/10.1016/j.dyepig.2004.12.010>.
- [19] S. Udayan, V.K. Ramachandran, M. Sebastian, P. Chandran, V.P.N. Nampoory, S. Thomas, Effect of DNA-CTMA complex on optical properties of LDS 821 dye, *Opt. Mater. (Amst.)* 69 (2017) 49–53, <https://doi.org/10.1016/j.optmat.2017.04.016>.
- [20] N. Nizomov, E.N. Kurtaliev, S.N. Nizamov, G. Khodjayev, Spectral-luminescent study of the interaction of some styrylcyanine dyes with bovine serum albumin and DNA in aqueous solutions, *J. Mol. Struct.* 936 (2009) 199–205, <https://doi.org/10.1016/j.molstruc.2009.07.040>.
- [21] V.B. Kovalska, I.O. Kocheshev, D.V. Kryvorotenko, A. Balanda, S.M. Yarmoluk, Studies on the spectral-luminescent properties of the novel homodimer styryl dyes in complexes with DNA, *J. Fluoresc.* 15 (2005) 215–219, <https://doi.org/10.1007/s10895-005-2620-5>.
- [22] C. Gao, S.Y. Liu, X. Zhang, Y.K. Liu, C. De Qiao, Z.E. Liu, Two-photon fluorescence and homodimeric imaging of two styryl heterocyclic dyes combined with DNA, *Spectrochim. Acta - Part A Mol. Biomol. Spectrosc.* 156 (2016) 1–8, <https://doi.org/10.1016/j.saa.2015.11.014>.
- [23] V.P. Tokar, M.Y. Losytskiy, T.Y. Ohulchanskyy, D.V. Kryvorotenko, V.B. Kovalska, A.O. Balanda, I.M. Dmytruk, V.M. Prokopets, S.M. Yarmoluk, V.M. Yashchuk, Styryl dyes as two-photon excited fluorescent probes for DNA detection and two-photon laser scanning fluorescence microscopy of living cells, *J. Fluoresc.* 20 (2010) 865–872, <https://doi.org/10.1007/s10895-010-0630-4>.
- [24] R. Tropcheva, N. Lesev, S. Danova, S. Stoitsova, S. Kaloyanova, Novel cyanine dyes and homodimeric styryl dyes as fluorescent probes for assessment of lactic acid bacteria cell viability, *J. Photochem. Photobiol. B Biol.* 143 (2015) 120–129, <https://doi.org/10.1016/j.jphotobiol.2015.01.002>.
- [25] N. Akbay, M.Y. Losytskiy, V.B. Kovalska, A.O. Balanda, S.M. Yarmoluk, The mechanism of benzothiazole styrylcyanine dyes binding with dsDNA: studies by spectral-luminescent methods, *J. Fluoresc.* 18 (2008) 139–147, <https://doi.org/10.1007/s10895-007-0252-7>.
- [26] D.V. Berdnikova, N.I. Sosnin, O.A. Fedorova, H. Ihmels, Governing the DNA-binding mode of styryl dyes by the length of their alkyl substituents—from intercalation to major groove binding, *Org. Biomol. Chem.* 16 (2018) 545–554, <https://doi.org/10.1039/c7ob02736b>.
- [27] A.Y. Lebedeva, O.A. Fedorova, V.B. Tsvetkov, V.Y. Grinberg, N.V. Grinberg, T. V. Burova, A.S. Dubovik, K.K. Babievsky, Y.V. Fedorov, Novel 18-crown-6-ether containing mono- and bisstyryl dyes derived from pyridine moiety as fluorescent dyes for non-covalent interaction with DNA, *Dyes Pigm.* 157 (2018) 80–92, <https://doi.org/10.1016/j.dyepig.2018.04.038>.
- [28] S. Brasselet, F. Cherioux, P. Audebert, J. Zyss, New octupolar star-shaped structures for quadratic nonlinear optics, *Chem. Mater.* 11 (1999) 1915–1920, <https://doi.org/10.1021/cm990093n>.
- [29] M.F. Pepitone, G.G. Jernigan, J.S. Melinger, O.K. Kim, Synthesis and characterization of donor-acceptor chromophores for unidirectional electron transfer, *Org. Lett.* 9 (2007) 801–804, <https://doi.org/10.1021/ol063000y>.
- [30] A.S. Brown, L.M. Bernal, T.L. Micotto, E.L. Smith, J.N. Wilson, Fluorescent neuroactive probes based on stilbazolium dyes, *Org. Biomol. Chem.* 9 (2011) 2142–2148, <https://doi.org/10.1039/c0ob00849d>.
- [31] R. Abagyan, M. Totrov, D. Kuznetsov, ICM—A new method for protein modeling and design: applications to docking and structure prediction from the distorted native conformation, *J. Comput. Chem.* 15 (1994) 488–506, <https://doi.org/10.1002/jcc.540150503>.
- [32] T.A. Halgren, Merck molecular force field. I. Basis, form, scope, parameterization, and performance of MMFF94, *J. Comput. Chem.* 17 (1996) 490–519, [https://doi.org/10.1002/\(SICI\)1096-987X\(199604\)17:5<490::AID-JCC1>3.0.CO;2-P](https://doi.org/10.1002/(SICI)1096-987X(199604)17:5<490::AID-JCC1>3.0.CO;2-P).
- [33] C. Møller, M.S. Plesset, Note on an approximation treatment for many-electron systems, *Phys. Rev.* 46 (1934) 618–622, <https://doi.org/10.1103/PhysRev.46.618>.
- [34] V. Barone, M. Cossi, Quantum calculation of molecular energies and energy gradients in solution by a conductor solvent model, *J. Phys. Chem. A* 102 (1998) 1995–2001, <https://doi.org/10.1021/jp9716997>.
- [35] U.C. Singh, P.A. Kollman, An approach to computing electrostatic charges for molecules, *J. Comput. Chem.* 5 (1984) 129–145, <https://doi.org/10.1002/jcc.540050204>.
- [36] C.I. Bayly, P. Cieplak, W.D. Cornell, P.A. Kollman, A well-behaved electrostatic potential based method using charge restraints for deriving atomic charges: the RESP model, *J. Phys. Chem.* 97 (1993) 10269–10280, <https://doi.org/10.1021/j100142a004>.
- [37] M.J. Frisch, G.W. Trucks, H.B. Schlegel, G.E. Scuseria, M.A. Robb, J.R. Cheeseman, G. Scalmani, V. Barone, B. Mennucci, G.A. Petersson, H. Nakatsuji, M. Caricato, X. Li, H.P. Hratchian, A.F. Izmaylov, J. Bloino, G. Zheng, J.L. Sonnenberg, M. Hada, M. Ehara, K. Toyota, R. Fukuda, J. Hasegawa, M. Ishida, T. Nakajima, Y. Honda, O. Kitao, H. Nakai, T. Vreven, J.A. Montgomery Jr., J.E. Peralta, F. Ogliaro, M. Bearpark, J.J. Heyd, E. Brothers, K.N. Kudin, V.N. Staroverov, R. Kobayashi, J. Normand, K. Raghavachari, A. Rendell, J.C. Burant, S.S. Iyengar, J. Tomasi, M. Cossi, N. Rega, J.M. Millam, M. Klene, J.E. Knox, J.B. Cross, V. Bakken, C. Adamo, J. Jaramillo, R. Gomperts, R.E. Stratmann, O. Yazyev, A.J. Austin, R. Cammi, C. Pomelli, J.W. Ochterski, R.L. Martin, K. Morokuma, V.G. Zakrzewski, G.A. Voth, P. Salvador, J.J. Dannenberg, S. Dapprich, A.D. Daniels, Ö. Farkas, J. B. Foresman, J.V. Ortiz, J. Cioslowski, D.J. Fox, Gaussian 09, Revision A.1, Gaussian, Inc., Allingford CT, 2009.
- [38] Y.A. Arnautova, A. Jagielska, H.A. Scheraga, A new force field (ECEPP-05) for peptides, proteins, and organic molecules, *J. Phys. Chem. B* 110 (2006) 5025–5044, <https://doi.org/10.1021/jp054994x>.
- [39] R. Abagyan, M. Totrov, Biased probability Monte Carlo conformational searches and electrostatic calculations for peptides and proteins, *J. Mol. Biol.* 235 (1994) 983–1002, <https://doi.org/10.1006/jmbi.1994.1052>.
- [40] M.J.D. Powell, Restart procedures for the conjugate gradient method, *Math. Program.* 12 (1977) 241–254, <https://doi.org/10.1007/BF01593790>.
- [41] M. Clark, R.D. Cramer, N. Van Opdenbosch, Validation of the general purpose tripos 5.2 force field, *J. Comput. Chem.* 10 (1989) 982–1012, <https://doi.org/10.1002/jcc.540100804>.
- [42] D.A. Case, I.Y. Ben-Shalom, S.R. Brozell, D.S. Cerutti, T.E. Cheatham III, V.W. D. Cruzeiro, T.A. Darden, R.E. Duke, D. Ghoreishi, M.K. Gilson, H. Gohlke, A. W. Goetz, D. Greene, R. Harris, N. Homeyer, Y. Huang, S. Izadi, A. Kovalenko, T. Kurtzman, T.S. Lee, S. LeGrand, P. Li, C. Lin, J. Liu, T. Luchko, R. Luo, D. J. Mermelstein, K.M. Merz, Y. Miao, G. Monard, C. Nguyen, H. Nguyen, I. Omelyan, A. Onufriev, F. Pan, R. Qi, D.R. Roe, A. Roitberg, C. Sagui, S. Schott-Verdugo, J. Shen, C.L. Simmerling, J. Smith, R. Salomon-Ferrer, J. Swails, R.C. Walker, J. Wang, H. Wei, R.M. Wolf, X. Wu, L. Xiao, D.M. York, P.A. Kollman, Amber 2018, University of California, San Francisco, 2018.
- [43] S. Izadi, A.V. Onufriev, Accuracy limit of rigid 3-point water models, *J. Chem. Phys.* 145 (2016) 74501, <https://doi.org/10.1063/1.4960175>.
- [44] M. Zgarbová, F.J. Luque, J. Šponer, T.E. Cheatham, M. Otyepka, P. Jurečka, Toward improved description of DNA backbone: revisiting epsilon and zeta torsion force field parameters, *J. Chem. Theory Comput.* 9 (2013) 2339–2354, <https://doi.org/10.1021/ct400154j>.
- [45] M. Zgarbová, J. Šponer, M. Otyepka, T.E. Cheatham, R. Galindo-Murillo, P. Jurečka, Refinement of the sugar-phosphate backbone torsion Beta for AMBER force fields improves the description of z- and B-DNA, *J. Chem. Theory Comput.* 11 (2015) 5723–5736, <https://doi.org/10.1021/acs.jctc.5b00716>.
- [46] A. Onufriev, D.A. Case, D. Bashford, Effective born radii in the generalized Born approximation: the importance of being perfect, *J. Comput. Chem.* 23 (2002) 1297–1304, <https://doi.org/10.1002/jcc.10126>.
- [47] L. Martínez, R. Andrade, E.G. Birgin, J.M. Martínez, PACKMOL: A package for building initial configurations for molecular dynamics simulations, *J. Comput. Chem.* 30 (2009) 2157–2164, <https://doi.org/10.1002/jcc.21224>.
- [48] S.H. Li, X. Xu, Y. Zhou, Q. Zhao, Y. Liu, Reversibly tunable white-light emissions of styrylpyridiniums with cucurbiturils in aqueous solution, *Org. Lett.* 19 (2017) 6650–6653, <https://doi.org/10.1021/acs.orglett.7b03377>.
- [49] Y. Huang, T. Cheng, F. Li, C.H. Huang, T. Hou, A. Yu, X. Zhao, X. Xu, Photophysical studies on the mono- and dichromophoric hemicyanine dyes I. Photoelectric conversion from the dye modified ITO electrodes, *J. Phys. Chem. B* 106 (2002) 10020–10030, <https://doi.org/10.1021/jp020876n>.
- [50] E.V. Tulyakova, O.A. Fedorova, Y.V. Fedorov, G. Jonusauskas, A.V. Anisimov, Effect of arrangement of the styryl fragment on the optical properties and complexation of mono- and bis(styryl)-substituted N-methylpyridinium perchlorates containing benzo-15-crown-5 ether moieties, *Russ. Chem. Bull.* 56 (2007) 2166–2174, <https://doi.org/10.1007/s11172-007-0341-4>.
- [51] E.V. Tulyakova, O.A. Fedorova, Y.V. Fedorov, G. Jonusauskas, A.V. Anisimov, Spectroscopic study of mono- and bis(styryl) dyes of the pyridinium series containing azathiocrown ether residue, *J. Phys. Org. Chem.* 21 (2008) 372–380, <https://doi.org/10.1002/poc.1349>.
- [52] A. Olaya-Castro, G.D. Scholes, Energy transfer from Förster-Dexter theory to quantum coherent light-harvesting, *Int. Rev. Phys. Chem.* 30 (2011) 49–77, <https://doi.org/10.1080/0144235X.2010.537060>.
- [53] D. Sahoo, P. Bhattacharya, S. Chakravorty, Quest for mode of binding of 2-(4-(dimethylamino)styryl)-1-methylpyridinium iodide with calf thymus DNA, *J. Phys. Chem. B* 114 (2010) 2044–2050, <https://doi.org/10.1021/jp910766q>.
- [54] M.A. Ustimova, P.A. Chernikova, N.E. Shepel, Y.V. Fedorov, O.A. Fedorova, Effect of N-substituent in 4-styrylpyridinium dyes on their binding to DNA, *Mendeleev Commun.* 30 (2020) 217–219, <https://doi.org/10.1016/j.mencom.2020.03.029>.
- [55] Alison Rodger, Bengt Nordén Circular Dichroism and Linear Dichroism, Oxford University Press, New York, 1997 ch. 2.
- [56] M. Eriksson, B. Nordén, Linear and circular dichroism of drug-nucleic acid complexes, *Methods Enzymol.* 340 (2001) 68–98, [https://doi.org/10.1016/S0076-6879\(01\)40418-6](https://doi.org/10.1016/S0076-6879(01)40418-6).
- [57] B. Nordén, F. Tjerneld, Structure of methylene blue–DNA complexes studied by linear and circular dichroism spectroscopy, *Biopolymers* 21 (1982) 1713–1734, <https://doi.org/10.1002/bip.360210904>.
- [58] H.K. Kim, J.M. Kim, S.K. Kim, A. Rodger, B. Nordén, Interactions of intercalative and minor groove binding ligands with triplex poly(dA)·[poly(dT)]<sub>2</sub> and with duplex poly(dA)·poly(dT) and poly[d(A-T)]<sub>2</sub> studied by CD, LD, and normal absorption, *Biochemistry* 35 (1996) 1187–1194, <https://doi.org/10.1021/bi951913m>.
- [59] B. Nordén, T. Kurucsev, Analysing DNA complexes by circular and linear dichroism, *J. Mol. Recognit.* 7 (1994) 141–155, <https://doi.org/10.1002/jmr.300070211>.
- [60] A. Rodger, S. Taylor, G. Adlam, I.S. Blagbrough, I.S. Haworth, Multiple DNA binding modes of anthracene-9-carbonyl-N1-spermine, *Bioorg. Med. Chem. Lett.* 3 (1995) 861–872, [https://doi.org/10.1016/0968-0896\(95\)00086-V](https://doi.org/10.1016/0968-0896(95)00086-V).
- [61] J.L. Seifert, R.E. Connor, S.A. Kushon, M. Wang, B.A. Armitage, Spontaneous assembly of helical cyanine dye aggregates on DNA nanotemplates, *J. Am. Chem. Soc.* 121 (1999) 2987–2995, <https://doi.org/10.1021/ja984279j>.
- [62] K. Nakanishi, N. Berova, R.W. Woody, Circular Dichroism: Principles and Applications, VCH Publishers, New York, 1994.
- [63] S.K. Kim, B. Nordén, Methyl green, *FEBS Lett.* 315 (1993) 61–64, [https://doi.org/10.1016/0014-5793\(93\)81133-K](https://doi.org/10.1016/0014-5793(93)81133-K).
- [64] S. Neidle, DNA minor-groove recognition by small molecules, *Nat. Prod. Rep.* 18 (2001) 291–309, <https://doi.org/10.1039/a705982e>.